UNC-45A is required for neurite extension via controlling NMII activation

Yoshie Iizuka[a,†], Ashley Mooneyham[a,†], Andrew Sieben[a], Kevin Chen[b], Makayla Maile[a], Raffaele Hellweg[c], Florian Schütz[c], Kebebush Teckle[a], Timothy Starr[a], Venugopal Thayanithy[d], Rachel Isaksson Vogel[a], Emil Lou[d], Michael K. Lee[e], and Martina Bazzaro[a,*]

[a]Masonic Cancer Center and Department of Obstetrics, Gynecology and Women's Heath, [d]Division of Hematology, Oncology and Transplantation, and [e]Department of Neuroscience, University of Minnesota Twin Cities, Minneapolis, MN 55455; [b]Department of Biology, University of Maryland, Baltimore, MD 21250; [c]Breast Unit, University of Heidelberg, 69120 Heidelberg, Germany

ABSTRACT **UNC-45A is a highly conserved member of the UNC-45/CRO1/She4p family of proteins, which act as chaperones for conventional and nonconventional myosins. NMII mediates contractility and actin-based motility, which are fundamental for proper growth cone motility and neurite extension. The presence and role of UNC-45A in neuronal differentiation have been largely unknown. Here we demonstrate that UNC-45A is a novel growth cone–localized, NMII-associated component of the multiprotein complex regulating growth cone dynamics. We show that UNC-45A is dispensable for neuron survival but required for neurite elongation. Mechanistically, loss of UNC-45A results in increased levels of NMII activation. Collectively our results provide novel insights into the molecular mechanisms of neurite growth and define UNC-45A as a novel and master regulator of NMII-mediated cellular processes in neurons.**

Monitoring Editor
Paul Forscher
Yale University

Received: Jul 18, 2016
Revised: Mar 15, 2017
Accepted: Mar 21, 2017

INTRODUCTION

Neural development, including differentiation, migration, and neurite guidance, is a tightly regulated process under the control of cytoskeletal machinery. Neurite growth takes place at the highly motile tip of the neurite, the growth cone. A number of actin-associated proteins, including Wiskott–Aldrich syndrome protein (WASP), WASP-family verprolin-homologous family proteins, Arp2/3 complex, cofilin, and nonmuscle myosin II (NMII) participate in the stepwise cytoskeletal reorganization that is requisite for neurite extension and guidance (Lin *et al.*, 1994, 1996; Suter and Forscher, 2000; Lowery and Van Vactor, 2009; Spillane *et al.*, 2012; Ganguly *et al.*, 2015; Katsuno *et al.*, 2015).

In the transition zone of the growth cone, NMII-dependent contraction promotes F-actin retrograde flow and contributes to maintain the balance between actin polymerization and depolymerization, which is at the base of the idling of the growth cone engine (Schaar and McConnell, 2005; Lowery and Van Vactor, 2009; Vallee *et al.*, 2009). Consequently modulation of NMII dynamics has profound effects on cytoskeleton organization and cellular functions, including neurite growth (Lin *et al.*, 1996; Gallo *et al.*, 2002). NMII contractile properties depend on its ability to functionally bind and interact with actin (Vicente-Manzanares *et al.*, 2007, 2009). In this scenario, pharmacological inhibition of NMII with the general myosin II inhibitor blebbistatin results with an imbalance in the actin treadmilling and causes neurite extension (Limouze *et al.*, 2004; Cai *et al.*, 2010).

UNC-45A, a member of the UCS protein family (UNC-45/CRO1/She4p), is a NMII cochaperone required for motor protein assembly (Barral *et al.*, 1998, 2002; Hutagalung *et al.*, 2002; Price *et al.*, 2002; Lee *et al.*, 2014; Ni and Odunuga, 2015). We and others showed that UNC-45A is also required for a variety of NMII-mediated functions in mammalian cells, including motility, adhesion, exocytosis, and cytokinesis (Price *et al.*, 2002; Hoppe *et al.*, 2004; Bazzaro *et al.*, 2007; Guo *et al.*, 2011; Iizuka *et al.*, 2015; Jilani *et al.*, 2015). Mechanistically, UNC-45A has been suggested to promote stable NMII folding via binding with the myosin head,

This article was published online ahead of print in MBoC in Press (http://www.molbiolcell.org/cgi/doi/10.1091/mbc.E16-06-0381) on March 29, 2017.

†These authors contributed equally to this work.

*Address correspondence to: Martina Bazzaro (mbazzaro@umn.edu).

Abbreviations used: Arp, actin-related protein; F-actin, filamentous actin; FBS, fetal bovine serum; NMII, nonmuscle myosin II; PND1, postnatal day 1; sh, short hairpin; WASP, Wiskott–Aldrich syndrome protein.

thereby affecting the levels of available NMII to form NMII–actin complexes (Shi and Blobel, 2010; Guo *et al.*, 2011; Iizuka *et al.*, 2015).

Given the crucial role for NMII in regulating growth cone dynamics, we sought to investigate whether and how its cochaperone UNC-45A is necessary for neuronal differentiation. In this study, we show that UNC-45A is localized at the growth cone of neurons, where it binds to and colocalizes with both NMIIA and NMIIB. We also show that UNC-45A is dispensable for neuronal cells survival but crucial for neurite differentiation, as UNC-45A knockdown interferes with elongation of neurites. Furthermore, rescue of UNC-45A was able to restore neurite outgrowth in neuronal cells. Mechanistically, we show that loss of UNC-45A results in increased levels of phosphorylation of NMII light chain, which is compatible with an increase in NMII contractility and suggestive of increased F-actin retrograde flow at the growth cone.

RESULTS

UNC-45A is expressed in neurons and enriched in the growth cones

We previously showed that UNC-45A is a cytoskeletal-associated protein involved in regulating the NMII-associated function of cytokinesis and cell motility in cancer cells (Bazzaro *et al.*, 2007). More recently, we showed that UNC-45A promotes the NMII-associated cytoskeletal reorganization required during cell secretion (Iizuka *et al.*, 2015). Thus we sought to investigate whether UNC-45A plays a role in neuronal development. To this end, we first determined UNC-45A protein levels and subcellular localization in neuronal cell lines and primary neurons. Specifically, cell lysates from N2a and SH-SY5Y mouse and human neuroblastoma cell lines and cortical neurons dissected from postnatal day 1 (PND1) C57BL/6 mice were subjected to Western blot analysis using a monoclonal antibody (mAb) against UNC-45A. As shown in Figure 1A, UNC-45A is expressed in both neuronal cell lines and primary neurons.

Next we monitored the subcellular localization of UNC-45A in differentiated N2a and SH-SY5Y neuroblastoma cell lines, as well as in PND1 cortical neurons. Specifically, N2a cells were differentiated over a period of 4 d by exposing them to reduced (10 to 0.5%) fetal bovine serum (FBS) concentration, SH-SY5Y cells were differentiated over a period of 6 d by exposing them to 1 μM retinoic acid, and PND1 cortical neurons were differentiated over a period of 3 d by culturing them in supplemented Neurobasal medium**.** Differentiation resulted, with cells having a main long neurite and several shorter neurites. This is consistent with the pattern of neuronal differentiation observed in vivo. Immunofluorescence microscopy analysis revealed that UNC-45A is present in the growth cone of N2a (Figure 1B), SH-SY5Y (Figure 1C), and PND1 (Figure 1D) cells. Specificity of UNC-45A immunostaining was confirmed by performing the staining after UNC-45A knockdown (Supplemental Figure S1).

UNC-45A knockdown results in viable neurons with unaltered morphology

With the goal of investigating a possible role for UNC-45A during neurite growth, we first sought to evaluate the feasibility of UNC-45A knockdown in neuronal cell lines and PND1 cortical neurons and its effect on cell viability and morphology. To this end, UNC-45A was knocked down via lentiviral-mediated delivery of short hairpin RNAs (shRNAs) targeting multiple UNC-45A regions in N2a, SH-SY5Y, and PND1 neurons, and the efficiency of UNC-45A knockdown was evaluated by Western blot analysis. UNC-45A knockdown resulted in reduction of UNC-45A expression up to ~70% in N2a cells and ~50% in SH-SY5Y cells when measured 48 h postinfection (Figure 2, A and B, respectively). UNC-45A knockdown in PND1 cortical neurons also resulted in efficient reduction in protein expression levels, which was detectable as early as 2 d postinfection (D2), with reduction of the UNC-45A expression up to ~80% by D4 (Figure 2C).

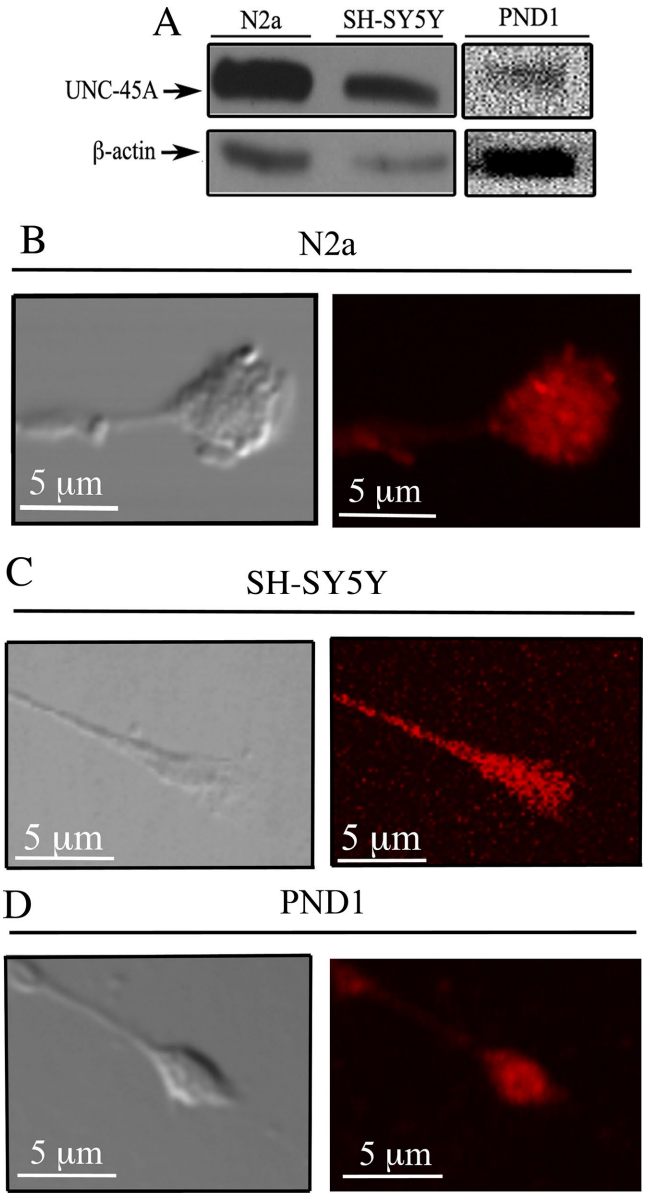

FIGURE 1: UNC-45A is expressed in neurons and localized in the growth cone. (A) Western blot analysis of UNC-45A in lysates from N2a and SH-SY5Y neuroblastoma cell lines and PND1 cortical neurons. β-Actin was used as loading control. (B) Differentiated N2a cells were stained using an anti–UNC-45A antibody followed by Texas Red–conjugated anti-mouse IgG and analyzed by phase contrast (left) and fluorescence (right) microscopy. (C) Differentiated SH-SY5Y cells were stained using an anti-UNC-45A antibody followed by Texas Red–conjugated anti-mouse IgG and analyzed by phase contrast (left) and fluorescence (right) microscopy. (D) Differentiated PND1 cortical neurons were stained using an anti-UNC-45A antibody followed by Texas Red–conjugated anti-mouse IgG and analyzed by phase contrast (left) and fluorescence (right) microscopy.

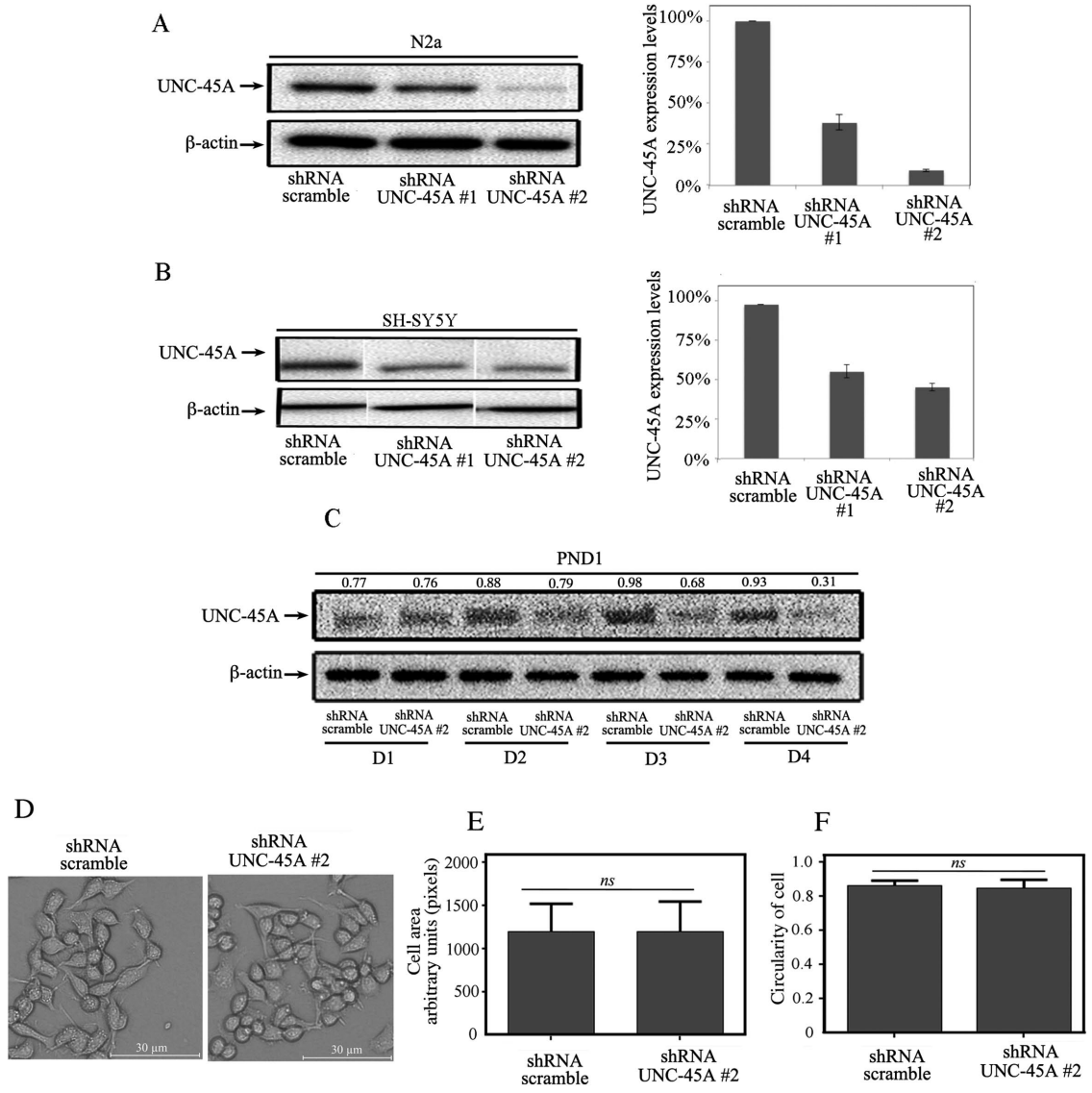

FIGURE 2: Lentiviral-mediated delivery of shRNA-UNC-45A results in efficient UNC-45A knockdown in neuronal cells without affecting their viability. (A) Left, UNC-45A expression levels evaluated via Western blot analysis in lysates of N2a cells 48 h after transduction with either shRNA-scramble or shRNA targeting two different UNC-45A regions (#1 and #2). β-Actin was used as a loading control. Right, quantification of percentage of UNC-45A expression normalized to β-actin. (B) Left, UNC-45A expression levels evaluated via Western blot analysis in lysates of SH-SY5Y cells on transduction with either shRNA-scramble or shRNA targeting two different UNC-45A regions (#1 and #2). β-Actin was used as a loading control. Right, quantification of percentage of UNC-45A expression normalized to β-actin. (C) UNC-45A expression levels evaluated via Western blot analysis in lysates of PND1 cortical neurons after transduction with either shRNA-scramble or shRNA targeting UNC-45A (#2). Analysis was performed at D1–D4 postinfection. β-Actin was used as a loading control. Numbers indicate UNC-45A/β-actin ratio. (D) Stable N2a cells expressing either scramble or UNC-45A knockdown (#2) evaluated for their morphology via phase contrast microscopy. (E) Cell area evaluated in shRNA-scramble vs. UNC-45A–knockdown (#2) N2a cells. Area is expressed as arbitrary units (pixels) and calculated using ImageJ software. (F) Cell shape (circularity) evaluated in shRNA-scramble vs. UNC-45A knockdown (#2) N2a cells. Circularity of the cell was defined as the ratio between the area of the cell and its perimeter ($4\pi \times \text{area/perimeter}^2$). The ratio ranges from 0 to 1, with 1 indicating a perfect circle and values progressing toward 0 representing an increasingly elongated shape.

Next we investigated whether loss of UNC-45A would result in loss of cell viability or alteration in cellular morphology in undifferentiated cells. To this end, undifferentiated N2a cells stably expressing shRNA-scramble or shRNA-UNC-45A (#2) were analyzed under light microscopy for general cell appearance, including cell size and shape. As shown in Figure 2D, we did not observe significant differences in cell morphology between UNC-45A knockdown and control. Furthermore, analysis of cell morphology did not reveal significant differences in terms of cell area (Figure 2E) or shape (Figure 2F). Similar results were obtained with PND1 cortical neurons (unpublished data). Collectively the results suggest that the dramatic reduction in UNC-45A protein levels does not compromise neuronal cell viability nor compromise the overall morphology of undifferentiated neurons.

Loss of UNC-45A hinders the capacity of neurons to differentiate and form a main neurite

Having established that UNC-45A knockdown results in viable cells, we next investigated whether UNC-45A is required for cell differentiation and more specifically for neurite growth. To this end, N2a cells stably expressing either shRNA-scramble or shRNA targeting two different UNC-45A regions (#1 and #2) were exposed to low serum concentrations (0.5%) for 48 h, followed by fixation and visualization under phase contrast microscopy. As shown in Figure 3A, UNC-45A knockdown severely inhibited the ability of N2a cells to differentiate and produce neurites. Quantification of the main neurite/soma ratio for N2a and SH-SY5Y UNC-45A knockdowns, respectively, is given in Figure 3, B and C.

Next we investigated whether a similar effect could be observed in primary cortical neurons. To this end, PND1 cortical neurons from C57BL/6 mice were infected at day in vitro 1 (DIV 1), and main neurite length was monitored under phase contrast microscopy at D1–D4. As shown in Figure 3D, UNC-45A knockdown resulted in statistically significant reduction in main neurite length, which was observable as early as D2 and progressively increased to reach its

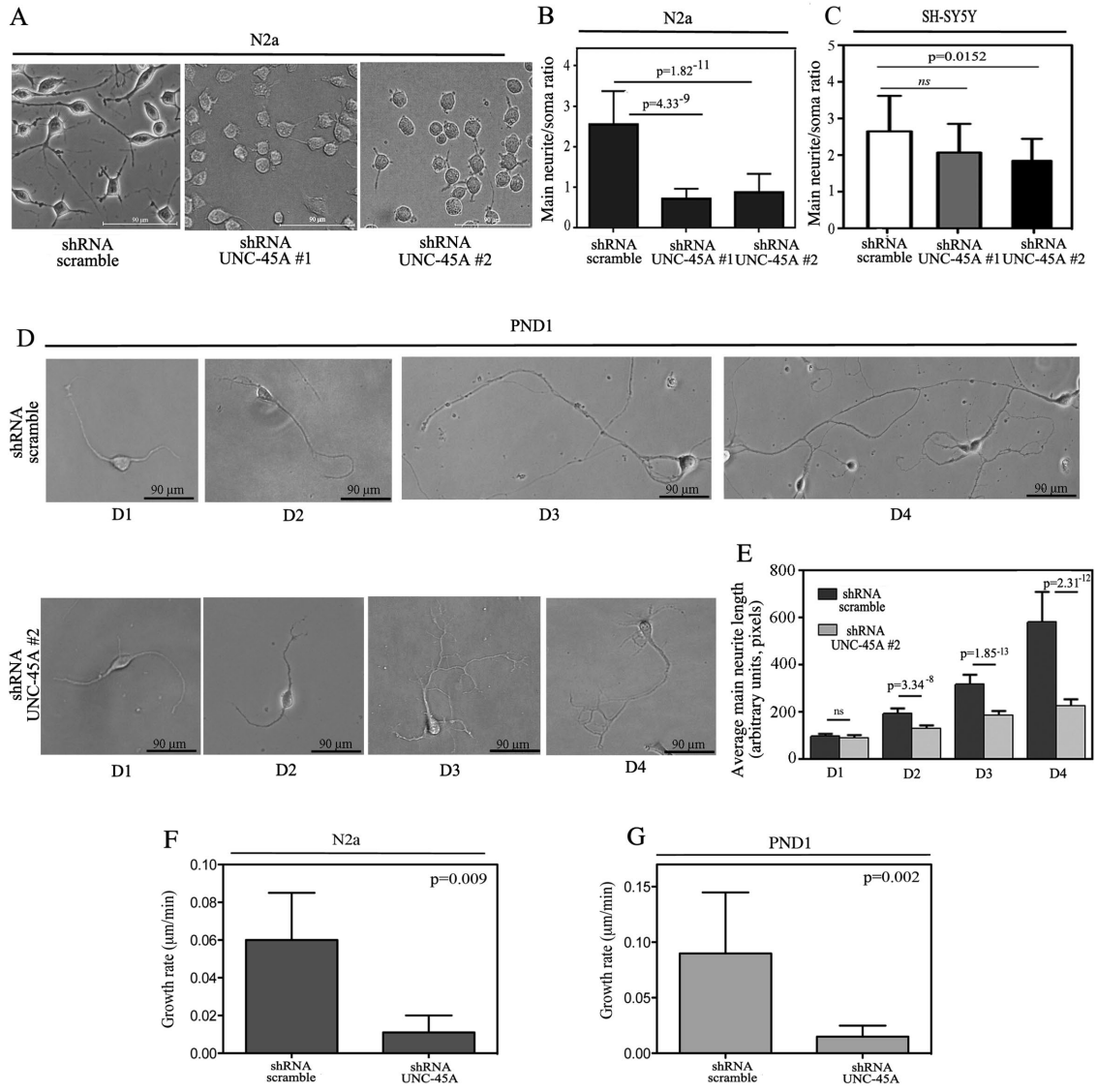

FIGURE 3: Loss of UNC-45A prevents neurite elongation. (A) N2a cells transduced with either shRNA-scramble or shRNA targeting two different UNC-45A regions (#1 and #2) and differentiated in presence of 0.5% of FBS over 48 h. Per each condition, soma and main neurite lengths were visualized and evaluated under phase contrast microscopy. (B) Evaluation of main neurite/soma ratio in scramble vs. UNC-45A–knockdown N2a cells. Average of three independent experiments. (C) Evaluation of main neurite/body ratio in scramble vs. UNC-45A knockdown in SH-SY5Y cells. Average of three independent experiments. (D) PND1 cortical neurons were transduced with either shRNA-scramble or shRNA-UNC-45A (#2). Per each condition, neurite length was visualized and evaluated under phase contrast microscopy at D1–D4 postinfection. (E) Evaluation of main neurite length in scramble vs. UNC-45A PND1 knockdown cells. Average of three independent experiments. (F) Growth rate of main neurite in N2a cells scramble or UNC-45A knockdown expressed as micrometers/minute. A minimum of four neurons were analyzed per each condition. (G) Growth rate of main neurite in PND1 scramble or UNC-45A knockdown expressed as micrometers/minute. A minimum of four neurons were analyzed per each condition.

peak at D4. Quantification of the average main neurite length in control versus UNC-45A–knockdown PND1 neurons is given in Figure 3E.

UNC-45A knockdown interferes with neurite elongation

The formation of the neurite is an initial event during the polarization of neurons. Thus, to establish whether loss of UNC-45A plays a role during neuronal polarization, we performed time-lapse microscopy imaging of N2a stably expressing either shRNA-scramble or shRNA targeting UNC-45A (#2). Specifically, infected cells were exposed to low concentration of serum (0.5%), and neuronal polarization and neurite extension were visualized via time-lapse microscopy over 3 d. As shown in Supplemental Video S1, N2a cells infected with shRNA-scramble retain the capacity to polarize and form growing neurites. On the contrary, ~70% of N2a cells expressing shRNA directed against UNC-45A showed a marked increase in number of neurites but failed to commit to form a main one (Supplemental Video S2). Taken together, these results suggest that the transition from neurites to main neurite seems to be inhibited. Next we sought to determine whether loss of UNC-45A hinders the extension of already formed neurites. For this, we took advantage of the observed delay in down-regulation of UNC-45A protein in PND1 cortical neurons after infection (Figure 2C). Under these conditions, decrease in UNC-45A protein levels occurs when neurons are already semidifferentiated and have produced a main neurite. As shown in Supplemental Video S3, PND1 cortical neurons infected with shRNA-scramble retained their capacity to form a defined, main neurite. On the contrary, neurites from PND1 cortical neurons infected with shRNA targeting UNC-45A had slower growth and shorter length (Supplemental Video S4). Growth rate for N2a or PND1 scramble and UNC-45A–knockdown cells is given in Figure 3, F and G, respectively. Taken together, the results suggest that UNC-45A knockdown interferes with neurite elongation.

Rescue of UNC-45A restores neurite growth in UNC-45A–knockdown N2a cells

To confirm that UNC-45A is necessary during neurite growth, we designed a rescue experiment in which UNC-45A was reexpressed in stable UNC-45A–knockdown N2a cell lines. Specifically, shRNA UNC-45A #2 knockdown N2a cells were transduced with either empty FLAG vector or vector expressing FLAG-tagged UNC-45A, and the efficiency of protein rescue was evaluated by Western blot analysis (Figure 4A). Next knockdown N2A cells infected with either empty vector (+empty vector) or vector expressing FLAG-tagged UNC-45A (+UNC-45A) were exposed to low serum concentrations (0.5%) for 48 h, followed by fixation and visualization under phase contrast microscopy. As shown in Figure 4B, UNC-45A rescue resulted in N2a cells having neurites statistically significantly longer than control (+empty vector) and similar to those in shRNA-scramble cells. Quantification of the main neurite/soma ratio for UNC-45A rescue versus controls is given in Figure 4C.

UNC-45A colocalizes with and binds to NMIIA and NMIIB

We and others previously showed that in mammalian cells, UNC-45A plays a crucial role in controlling NMII-associated functions (Price *et al.*, 2002; Hoppe *et al.*, 2004; Guo *et al.*, 2011; Ni *et al.*, 2011; Iizuka *et al.*, 2015; Jilani *et al.*, 2015). Furthermore, UNC-45A was previously shown to bind to both NMIIA and NMIIB in cancer cells (Guo *et al.*, 2011). Given the key role of NMII in driving neuronal differentiation and neurite formation, we initially tested the hypothesis that in neurons, UNC-45A is a binding partner of NMII. To this end, we first evaluated the UNC-45A subcellular localization in differentiated neurons with respect to NMIIA. Specifically, differentiated N2a cells were fixed and stained with UNC-45A and NMIIA antibodies, and the relative subcellular localization was investigated via double immunofluorescence analysis. Our results show that UNC-45A partially overlaps with NMIIA in both cell soma and growth cone of differentiated N2a cells (Figure 5A). Next we

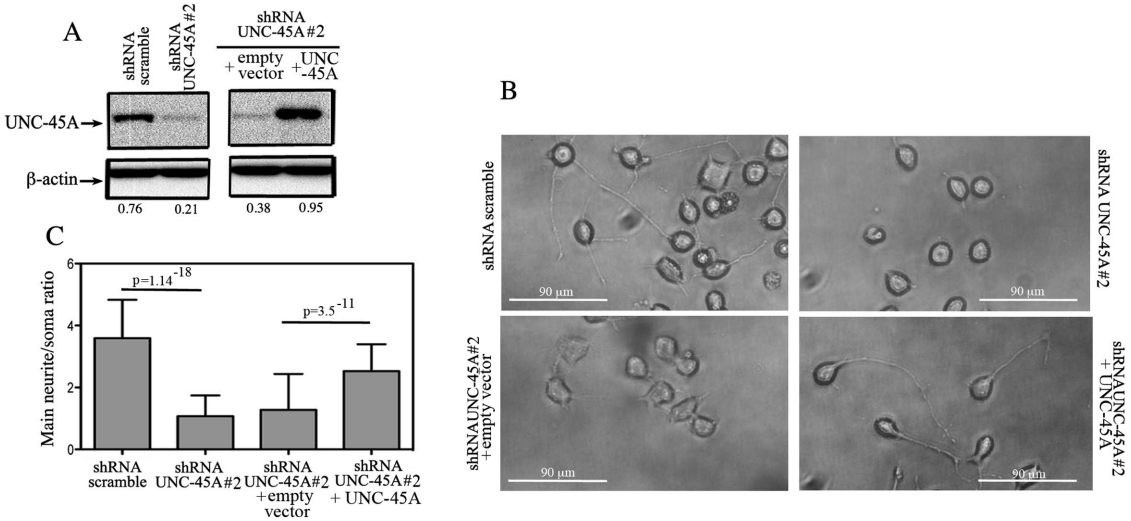

FIGURE 4: Rescue of UNC-45A restores neurite growth in UNC-45A–knockdown N2a cells. (A) UNC-45A expression levels evaluated via Western blot analysis in lysates of UNC-45A knockdown (shRNA UNC-45A #2) N2A cells infected with either empty vector (+empty vector) or vector expressing FLAG-tagged UNC-45A (+UNC-45A). β-Actin was used as a loading control. Numbers indicate the UNC-45A/β-actin ratio. (B) Scramble or UNC-45A–knockdown N2A cells infected with either empty vector or vector expressing UNC-45A were differentiated in the presence of 0.5% of FBS over 48 h. Per each condition, soma and main neurite lengths were visualized and evaluated under phase contrast microscopy. (C) Evaluation of main neurite/soma ratio per each condition. Average of three independent experiments.

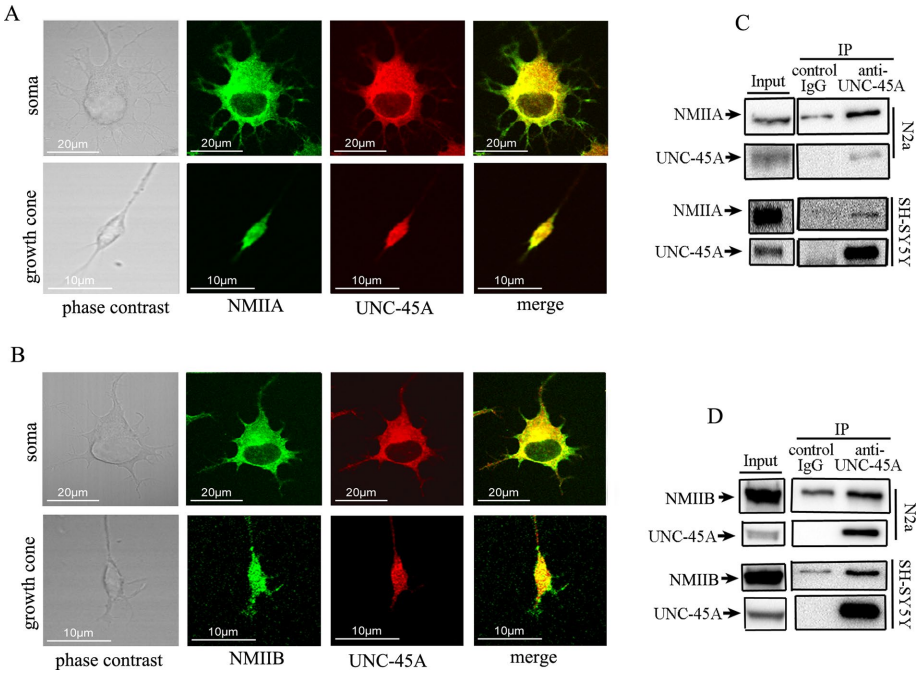

FIGURE 5: UNC-45A binds to and colocalizes with NMIIA and NMIIB in neurons. (A) Differentiated N2a cells were stained with anti–UNC-45A antibody followed by Texas Red–conjugated anti-mouse antibody (red) and anti-NMIIA antibody followed by an anti-rabbit FITC–conjugated secondary antibody (green). Stained cells were analyzed by confocal immunofluorescence microscopy. (B) Differentiated N2a cells were stained with anti–UNC-45A antibody followed by Texas Red–conjugated anti-rabbit antibody (red) and anti-NMIIB antibody followed by an anti-mouse FITC conjugated secondary antibody (green). Stained cells were analyzed by confocal immunofluorescence microscopy. (C) UNC-45A immunoprecipitated from lysates of N2a and SH-YH5Y cells with an anti-UNC-45A mAb. Coimmunoprecipitated NMIIA was detected by Western blot analysis using an anti-NMIIA polyclonal antibody. Immunoprecipitation with mouse IgG was performed as a control. (D) UNC-45A immunoprecipitated from lysates of N2a and SH-YH5Y cells with an anti–UNC-45A mAb. Coimmunoprecipitated NMIIB was detected by Western blot analysis using an anti-NMIIB polyclonal antibody. Immunoprecipitation with mouse IgG was performed as a control.

evaluated the UNC-45A subcellular localization in differentiated neurons with respect to NMIIB. Specifically, differentiated N2a cells were fixed and stained with UNC-45A and NMIIB antibodies, and the relative subcellular localization was investigated via double immunofluorescence analysis. Our results show that UNC-45A partially overlaps with NMIIB in both cell soma and growth cone of differentiated N2a cells (Figure 5B).

Next we biochemically tested whether UNC-45A coimmunoprecipitates with either or both NMIIA and NMIIB in neurons. To this end, we immunoprecipitated lysates from N2a and SH-SY5Y neuroblastoma cell lines with an anti–UNC-45A mAb and evaluated binding to NMIIA and NMIIB by Western blot analysis. As shown in Figure 5, UNC-45A coimmunoprecipitates with both NMIIA (Figure 5C) and NMIIB (Figure 5D). Taken together, the results suggest that UNC-45A is a likely candidate for mediating some of the NMII-associated functions in neuronal cells.

UNC-45A knockdown does not affect NMIIA or NMIIB levels or their subcellular localization

Neuronal differentiation is very sensitive to appropriate levels and subcellular localization of NMII (Vallee *et al.*, 2009). Thus the inhibition of neurite growth in neuroblastoma cell lines and PND1 cortical neurons after UNC-45A knockdown could be associated with reduction in NMII expression levels or its mislocalization within neuronal cells. Therefore we evaluated NMIIA and NMIIB expression levels in N2a UNC-45A–knockdown cells compared with controls. Specifically, we knocked down UNC-45A via lentiviral-mediated delivery of shRNAs targeting multiple UNC-45A regions in N2a cells and assessed the expression levels of NMIIA and NMIIB by immunoblot analysis. As shown in Figure 6, reduction of UNC-45A levels did not alter the levels of NMIIA (Figure 6A) or NMIIB (Figure 6B). Next we tested whether UNC-45A knockdown results in abnormal NMIIA and/or NMIIB subcellular localization in differentiating neurons. Specifically, we stained UNC-45A–knockdown N2a cells with an antibody against NMIIA and NMIIB and analyzed their growth cone localization via fluorescence microscopy. As shown in Figure 6, UNC-45A knockdown did not result with mislocalization of NMIIA (Figure 6C) or NMIIB (Figure 6D) in N2a cells on UNC-45A knockdown.

UNC-45A knockdown results in increased NMII phosphorylation levels

Because we did not observe any difference in NMIIA or NMIIB expression levels or their subcellular localization on UNC-45A knockdown (Figure 5), we next examined the effect of UNC-45A silencing on NMII activation. Specifically, we assessed phosphorylation levels of NMII light chain (Ser-19) by Western blot analysis in N2a cells infected with either shRNA-scramble or shRNA-UNC-45A (#1 and #2). As shown in Figure 7A (left), phosphorylation levels of NMII light chain were higher in UNC-45A–knockdown N2a cells than with control. Quantification of p-NMII light chain/β-actin ratio is given in Figure 7A (right). Next we investigated whether a similar effect could be observed in primary cortical neurons. To this end, we assessed phosphorylation levels of NMII light chain via Western blot analysis in PND1 neurons expressing shRNA-scramble or shRNA-UNC-45A (#2). Similar to N2a cells, we observed an increase in light chain phosphorylation in UNC-45A–knockdown PND1 cells compared with controls (Figure 7B, left). Quantification of p-NMII light chain/β-actin ratio is given in Figure 7B (right). To further support our findings of functional interaction between UNC-45A and NMII, we tested whether UNC-45A overexpression resulted in reduction in NMIIA phosphorylation levels. As shown in Figure 7C, overexpression of UNC-45A in N2a cells resulted in a decrease in NMIIA phosphorylation levels. Quantification of the p-NMII light chain/β-actin ratio is given in Figure 7C (right).

Increase in NMII activity after UNC-45A knockdown corresponds to an inhibition in neurite growth. This is consistent with previous observations that NMII inhibition promotes neurite extension (Kovács *et al.*, 2004; Allingham *et al.*, 2005; Hur *et al.*, 2011). Therefore we tested whether the effect of UNC-45A knockdown on main neurite growth can be antagonized by the addition of the general NMII inhibitor blebbistatin. Specifically, N2a cells expressing either shRNA-scramble or shRNA-UNC-45A were treated with either dimethyl sulfoxide (DMSO) (vehicle control) or 25 μM blebbistatin.

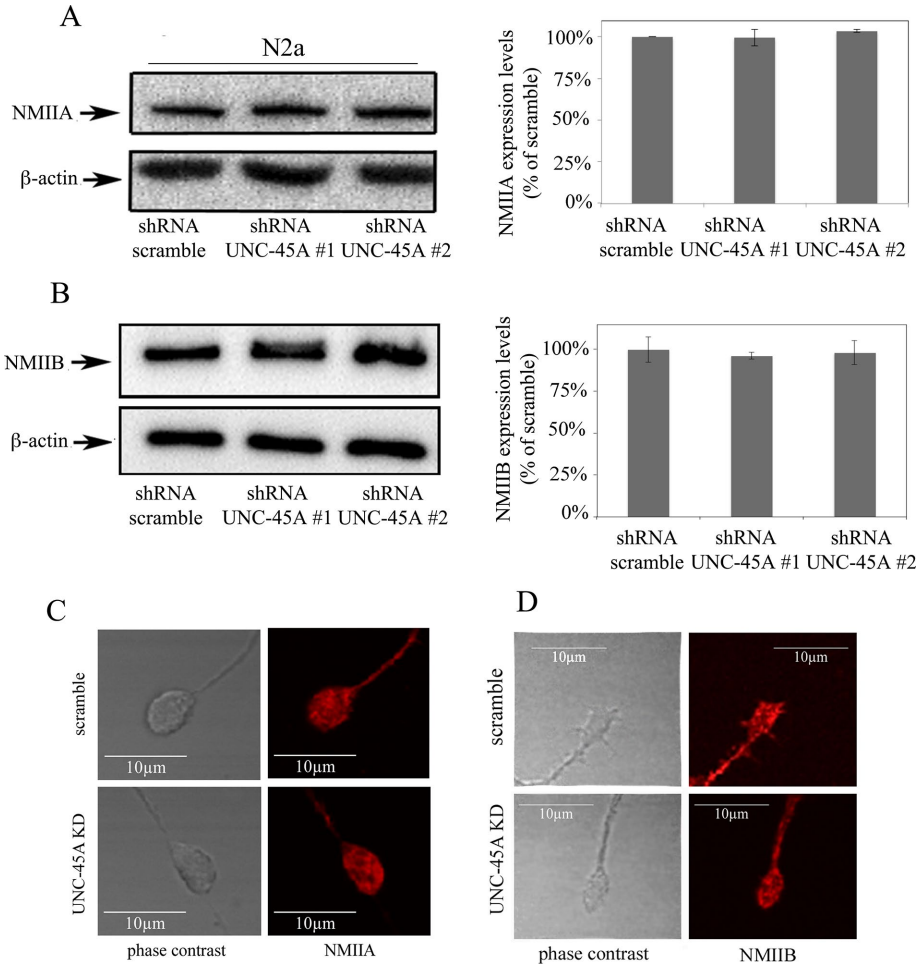

FIGURE 6: UNC-45A knockdown does not affect NMIIA and NMIIB levels or their subcellular localization at the growth cones. (A) Left, lysate of N2a cells expressing either scramble or UNC-45A knockdown (#1 and #2) was immunoblotted with an antibody against NMIIA. Equal protein loading was verified by using an antibody directed against β-actin. Right, quantification of residual NMIIA expression after UNC-45A knockdown. (B) Left, lysate of N2a cells expressing either scramble or UNC-45A knockdown (#1 and #2) was immunoblotted with an antibody against NMIIB. Equal protein loading was verified by using an antibody directed against β-actin. Right, quantification of residual NMIIB expression after UNC-45A knockdown. (C) Differentiated N2a cell expressing either shRNA-scramble or shRNA-UNC-45A#2 stained with an anti NMIIA antibody followed by Texas Red–conjugated anti-rabbit antibody (red) and analyzed by fluorescence microscopy. (D) Differentiated N2a cells expressing either shRNA-scramble or shRNA-UNC-45A#2 stained with an anti NMIIB antibody followed Texas Red–conjugated anti-rabbit antibody (red) and analyzed by fluorescence microscopy.

Neurite length was measured 24 h posttreatment. As shown in Figure 8A, blebbistatin treatment successfully rescued neurite extension in UNC-45A–silenced N2a cells. Quantitative analysis of neurite length in Figure 8B shows a nonsignificant difference in neurite length between blebbistatin-treated shRNA-scramble and shRNA-UNC-45A N2a cells. These data suggest that the loss of UNC-45A causes an increase in NMII activity that can subsequently be rescued on NMII inhibition.

DISCUSSION

In the transition zone of the growth cone, NMII-dependent contraction promotes F-actin retrograde flow and contributes to the idling of the growth cone engine (Forscher *et al.*, 1992; Cramer *et al.*, 1994; Lin *et al.*, 1996; Pollard *et al.*, 2000; Suter and Forscher, 2000). We and others previously showed that in mammalian cells, NMII-associated functions, including cytokinesis, cell motility, and exocytosis, depend on the presence of UNC-45A (Bazzaro *et al.*, 2007; Guo *et al.*, 2011; Jilani *et al.*, 2015). Given the role that UNC-45A plays in facilitating cytoskeletal dynamics through motor proteins, we initially investigated whether and where UNC-45A is expressed in neurons.

Here we show that UNC-45A is expressed in a panel of neuroblastoma cell lines, as well as in primary cortical neurons. Spatially, UNC-45A was found to localize in both the soma and the growth cone. Because growth cones are the nexus for neurite elongation, localization in this region suggests that UNC-45A plays a potential role in regulating neurite extension (Lowery and Vactor, 2009; Vicente-Manzanares *et al.*, 2009). Here we show that loss of UNC-45A in both neuroblastoma cell lines and primary cortical neurons results in impaired capacity of cells to commit to the formation of a main neurite.

Because previous studies showed that the cytoskeletal protein NMII depends on UNC-45A for proper folding and function, we tested UNC-45A and NMII interaction to determine whether disruption of this relationship impeded neuronal differentiation. Our colocalization and immunoprecipitation analyses confirm UNC-45A/NMIIA and UNC45A/NMIIB interaction in the neuronal context, similar to previous studies showing UNC-45A binding directly to NMIIA and NMIIB to facilitate folding and actin binding (Bazzaro *et al.*, 2007; Guo *et al.*, 2011). Both the loss of neuronal differentiation upon UNC-45A knockdown and the NMIIA/UNC-45A and NMIIB/UNC-45A colocalization and coimmunoprecipitation suggest that UNC-45A modulates neurite extension through NMII function or activity. We next hypothesized that UNC-45A knockdown could affect NMIIA and or NMIIB by altering their expression levels and/or subcellular localization. Here we show that loss of UNC-45A does not affect NMIIA or NMIIB expression in N2a cells, nor does it affect their subcellular localization.

The activated, functional form of NMII is a filamentous dimer that is assembled on phosphorylation of its regulatory light chain. Phosphorylation of NMII light chain prevents the interaction between the head and tail regions of NMII, unfurling NMII from its glomerular state and allowing cross-linkage between NMII and actin (Cross, 1988; Vicente-Manzanares *et al.*, 2009, Kiboku *et al.*, 2013). Here we show that loss of UNC-45A results in a marked increase in phosphorylation of NMII light chain in N2a and PND1 cells. This strongly suggests that UNC-45A contributes to neuron differentiation by regulating NMII activity through NMII light chain phosphorylation. Because NMIIA and NMIIB share the same light chain (Vicente-Manzanares *et al.*, 2009), it is possible that the increase in phosphorylation levels in the absence of UNC-45A occurs in NMIIA, NMIIB, or both.

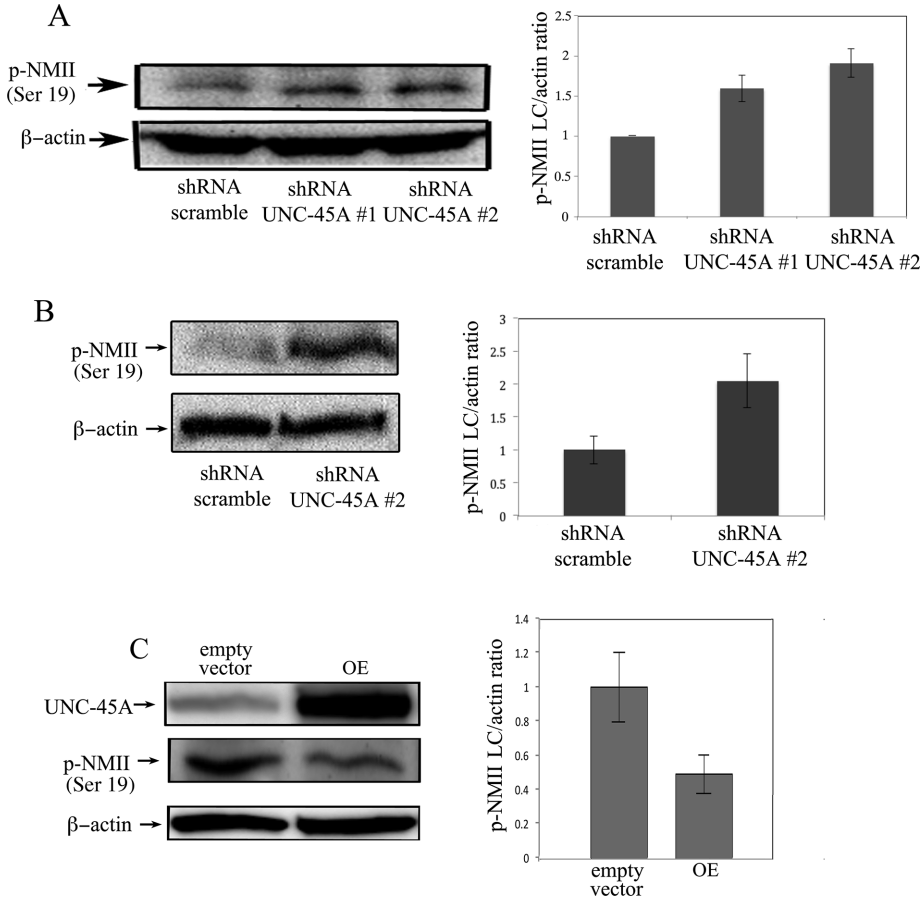

FIGURE 7: UNC-45A knockdown results in increased NMII phosphorylation levels. (A) Left, p-NMII (Ser-19) phosphorylation levels evaluated via Western blot analysis in lysates of N2a cells on transduction with either shRNA-scramble or shRNA targeting two different UNC-45A regions (#1 and #2). β-Actin was used as a loading control. Right, evaluation of the p-NMII light chain/β-actin ratio. (B) Left, p-NMII (Ser-19) phosphorylation levels evaluated via Western blot analysis in lysates of PND1 cortical neurons on transduction with either shRNA-scramble or shRNA targeting UNC-45A (#2). β-Actin was used as a loading control. Right, evaluation of the p-NMII light chain/β-actin ratio. (C) Left, UNC-45A and p-NMII light chain levels evaluated via Western blot analysis in lysates of N2a upon transduction with either empty vector or vector overexpressing FLAG-tagged UNC-45A (OE). β-Actin was used as a loading control. Right, evaluation of the p-NMII light chain/β-actin ratio.

NMII plays a crucial role in neurite extension by promoting the retrograde flow of F-actin within the transition zone of growth cones via a contracting myosin–actin network followed by severing of proximal actin bundles. In doing so, neurite extension is regulated via a balance between actin polymerization in the leading edge and retrograde actin flow in the transition zone (Medeiros *et al.*, 2006; Haviv *et al.*, 2008). By limiting the amount of NMII phosphorylation, UNC-45A controls NMII activation by reducing the amount of active, filamentous NMII. Our data suggest that loss of UNC-45A results in increased NMII contractile function and consequentially promotes higher rates of retrograde flow.

Blebbistatin is a general NMII inhibitor that has been shown to preferentially bind to NMII during its actin-detached state, preventing release of ADP and phosphate from its active site. As a result, NMII remains in a state of low actin affinity (Kovács *et al.*, 2004; Allingham *et al.*, 2005; Hur *et al.*, 2011). Here we show that blebbistatin treatment in N2a cells rescues neurite elongation regardless of UNC-45A expression. Despite an increase in active NMII, neurite extension is recued via interruption of NMII–actin complexes. Taken collectively, these data suggest that neuronal differentiation requires UNC-45A–associated control of filamentous NMII levels.

MATERIALS AND METHODS

Cell lines

The mouse N2a (Neuro-2a) neuroblastoma cell line and the human SH-SY5Y neuroblastoma cell line were purchased from the American Type Culture Collection.

Isolation of primary cortical neurons

Dissociated cortical neurons were prepared from PND1 C57BL/6 mice as described previously (Hilgenberg and Smith, 2007). Neurons were grown in Neurobasal medium supplemented with B-27, GlutaMAX, penicillin/streptomycin, mouse 5 ng/ml fibroblast growth factor-2 (FGF2), and 5 ng/ml platelet-derived growth factor-BB (PDGF-BB) on poly-L-lysine–coated plates or coverslip glass. At DIV 1, neurons were infected with lentiviral particles and used according to the manufacturer's instructions to silence UNC-45A.

Chemicals, antibodies, and plasmids

We used blebbistatin (Sigma-Aldrich), 5-(4,6-dichlorotriazinyl)aminofluorescein (ThermoFisher Scientific), anti–UNC-45A (Enzo Life Sciences), anti-NMIIA (BioLegend), anti–p-NMII LC (Ser-20; Abcam), anti-NMIIB (Santa Cruz Biotechnology), anti-actin (Sigma-Aldrich), Texas Red–goat anti-mouse immunoglobulin G (IgG), Texas Red–goat anti-rabbit IgG, fluorescein isothiocyanate (FITC)–donkey and anti-mouse IgG, peroxidase–goat anti-mouse IgG, peroxidase–goat anti-rabbit IgG (Jackson ImmunoResearch Laboratories), Neurobasal medium (Invitrogen), B-27 (Invitrogen), FGF2 (Invitrogen), mouse PDGHbb (Invitrogen), pRRLsinPPT, pMDLg/pRRE, pMD2.G, and pRSV-Rev plasmids (gifts from Alyson E. Fournier, Montreal Neurological Institute, Montreal, Canada), and Lenti-X concentrator (Clontech).

Modulation of UNC-45A expression levels in neuroblastoma cell lines and primary cortical neurons

For UNC-45A silencing in N2a, SH-YH5Y, and mouse cortical neuron cells, scramble and UNC-45A shRNAs (CTGGAAGATTACAGCAAAGCA [N2a and cortical neuron cells]/CTGGAAGATTACGACAAAGCA [SH-YH5Y cells] #1 and CCACCTCAAGCTGGAAGATTA #2) plus microRNA-30 oligonucleotides cassette were inserted into the green fluorescent protein–containing lentiviral pRRLsinPPT vector. The lentiviral vectors were cotransfected with lentiviral packaging plasmids (pMDLg/pRRE, pMD2.G, and pRSV-Rev) in HEK293T cells, and viral supernatants were concentrated using Lenti-X concentrator (Clontech) according to the manufacture's protocol. For UNC-45A rescue experiments, shRNA UNC-45A #2 knockdown N2A cells were infected with either empty vector (+empty vector) or vector expressing FLAG-tagged UNC-45A (+UNC-45A). For

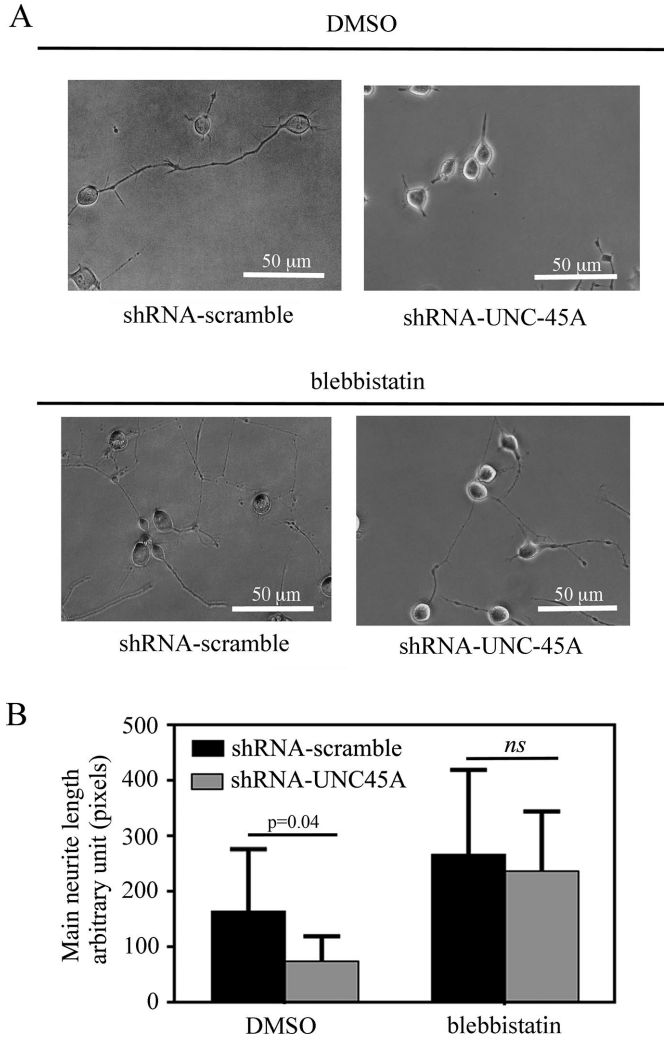

FIGURE 8: Blebbistatin treatment rescues neurite elongation in UNC-45A–silenced neurons. (A) N2a cells transduced with either shRNA-scramble or shRNA-UNC-45A and treated with DMSO (vehicle control) or 25 µM blebbistatin in DMEM with 0.5% FBS. Images were taken 24 h posttreatment using phase contrast microscopy. (B) Main neurite lengths were measured 24 h posttreatment using ImageJ analysis software. Data are represented as raw neurite length in arbitrary units. Average of three independent experiments.

UNC-45A–overexpression experiments, N2A cells were infected with either empty vector or vector overexpressing FLAG-tagged UNC-45A (OE).

Neuroblastoma cell line differentiation

Undifferentiated N2a and SH-YH5Y cells were cultured at 37°C with 5% CO_2 in DMEM with 10% FBS. Differentiation of N2a cell was induced over 3 d by reducing the FBS concentration from 10 to 0.5% and confirmed via phase contrast microscopy. Differentiation of SH-YH5Y cells was induced over 6 d by addition of 1 µM retinoic and confirmed via phase contrast microscopy.

Western blotting and coimmunoprecipitation

Cell lysates (20–40 µg) were subjected to Western blot analysis using the indicated antibodies. For coimmunoprecipitation, N2a and SH-YH5Y cells were lysed in lysis buffer (50 mM Tris, pH 7.4, 150 mM NaCl, 1% Nonidet P-40, 1× protease inhibitor mixture, 1× phosphatase inhibitor mixture), precleared, and precipitated with primary antibody and protein A/G beads. Samples were subjected to Western blot analysis using the specified antibodies.

Immunofluorescence microscopy

Cells were fixed with 30% ethanol/3.7% formaldehyde for 15 min at room temperature. After blocking with 5% bovine serum albumin in phosphate-buffered saline with 0.1% Tween-20, cells were stained with anti–UNC-45A, anti-NMIIA, or anti-NMIIB primary antibodies, followed by FITC- or Texas Red–conjugated secondary antibodies and analyzed via confocal fluorescence microscopy. Images were taken with a Nikon Eclipse T200 fluorescence microscope using a PlanApo VC 60×/1.4 ∞ 10.7 WD 0.13 oil lens (Nikon) and acquired using an NIS-Element F 3.3 camera and software. Alternatively, images were taken with an Olympus BX2 upright microscope equipped with a FluoView 1000 confocal scan head. A UPlanApo N 60×/1.42 NA objective and a pixel size of 0.082∞ was used. FITC was excited with a 488-nm laser, and emission was collected between 505 and 525 nm. For Texas Red, a 543-nm laser was used for excitation, and emission was collected between 560 and 660 nm. Images were taken with sequential excitation.

Measurement of neurite growth rate

Growth rate was calculated by measuring neurite length every 15 min over 24 h using ImageJ. The growth rate was defined as the average change in distance per minute over a 24-h period. A minimum of four neurons was analyzed per each condition.

Image analysis

Images were analyzed using ImageJ software. Circularity of the cell was defined as the ratio between the area of the cell and its perimeter ($4\pi \times \text{area/perimeter}^2$). The ratio ranges from 0 to 1, with 1 indicating a perfect circle and values progressing toward 0 representing an increasingly elongated shape. Phase contrast images of 3–30 neurons per field were analyzed with more than 200 neurons measured for each treatment using the ImageJ drawing tool. Neurite length was measured as either raw length or ratio between main neurite length and soma length understood as maximum diameter.

Live imaging

Live-imaging experiments were performed on an Axio Observer Z1 microscope equipped with an AxioCam CCD camera (Zeiss). Time-lapse acquisition was driven by Zen software. Live images were acquired every 15 min using a 20× phase objective. The cells were culturing with 5% CO_2, at 37°C in an Incubator XLmulti S1 (Pecon) using CO_2Module S and TempModule S (Zeiss).

Blebbistatin treatment

For N2a cells, shRNA-scramble or shRNA-UNC45A cells were treated with DMSO (vehicle control) or 25 µM blebbistatin in DMEM with 0.5% FBS (Straight *et al.*, 2003). The neurite lengths were measured 24 h posttreatment.

Statistical analysis

Results are reported as mean ± SD of three or more independent experiments. Unless otherwise indicated, statistical significance of difference was assessed by two-tailed Student's *t* using Prism version 4 (GraphPad, San Diego, CA) and Excel. The level of significance was set at $p < 0.05$.

ACKNOWLEDGMENTS

We are very grateful to the late Henry F. Epstein for his friendship and helpful discussion. We thank Paul C. Letourneau (University of Minnesota) for helpful discussion and Alyson E. Fournier (Montreal Neurological Institute) for the generous gift of plasmids. We thank Guillermo Marques (University of Minnesota Imaging Center) for assistance with image analysis. This work was supported by Department of Defense Ovarian Cancer Research Program Grant OC093424 and Randy Shaver Cancer Research Funds to M.B.

REFERENCES

Allingham JS, Smith R, Rayment I (2005). The structural basis of blebbistatin inhibition and specificity for myosin II. Nat Struct Mol Biol 12, 378–379.

Barral JM, Bauer CC, Ortiz I, Epstein HF (1998). Unc-45 mutations in Caenorhabditis elegans implicate a CRO1/She4p-like domain in myosin assembly. J Cell Biol 143, 1215–1225.

Barral JM, Hutagalung AH, Brinker A, Hartl FU, Epstein HF (2002). Role of the myosin assembly protein UNC-45 as a molecular chaperone for myosin. Science 295, 669–671.

Bazzaro M, Santillan A, Lin Z, Tang T, Lee MK, Bristow RE, Shih Ie M, Roden RB (2007). Myosin II co-chaperone general cell UNC-45 overexpression is associated with ovarian cancer, rapid proliferation, and motility. Am J Pathol 171, 1640–1649.

Cai Y, Rossier O, Gauthier NC, Biais N, Fardin MA, Zhang X, Miller LW, Ladoux B, Cornish VW, Sheetz MP (2010). Cytoskeletal coherence requires myosin-IIA contractility. J Cell Sci 123, 413–423.

Cramer LP, Mitchison TJ, Theriot JA (1994). Actin-dependent motile forces and cell motility. Curr Opin Cell Biol 6, 82–86.

Cross RA (1988). What is 10S myosin for? J Muscle Res Cell Motil 9, 108–110.

Forscher P, Lin CH, Thompson C (1992). Novel form of growth cone motility involving site-directed actin filament assembly. Nature 357, 515–518.

Gallo G, Yee HF Jr, Letourneau PC (2002). Actin turnover is required to prevent axon retraction driven by endogenous actomyosin contractility. J Cell Biol 158, 1219–1228.

Ganguly A, Tang Y, Wang L, Ladt K, Loi J, Dargent B, Leterrier C, Roy S (2015). A dynamic formin-dependent deep F-actin network in axons. J Cell Biol 210, 401–417.

Guo W, Chen D, Fan Z, Epstein HF (2011). Differential turnover of myosin chaperone UNC-45A isoforms increases in metastatic human breast cancer. J Mol Biol 412, 365–378.

Haviv L, Gillo D, Backouche F, Bernheim-Groswasser A (2008). A cytoskeletal demolition worker: myosin II acts as an actin depolymerization agent. J Mol Biol 375, 325–330.

Hilgenberg LG, Smith MA (2007). Preparation of dissociated mouse cortical neuron cultures. J Vis Exp 562, doi: 10.3791/562.

Hoppe T, Cassata G, Barral JM, Springer W, Hutagalung AH, Epstein HF, Baumeister R (2004). Regulation of the myosin-directed chaperone UNC-45 by a novel E3/E4-multiubiquitylation complex in C. elegans. Cell 118, 337–349.

Hur EM, Yang IH, Kim DH, Byun J, Saijilafu, Xu WL, Nicovich PR, Cheong R, Levchenko A, Thakor N, Zhou FQ (2011). Engineering neuronal growth cones to promote axon regeneration over inhibitory molecules. Proc Natl Acad Sci USA 108, 5057–5062.

Hutagalung AH, Landsverk ML, Price MG, Epstein HF (2002). The UCS family of myosin chaperones. J Cell Sci 115, 3983–3990.

Iizuka Y, Cichocki F, Sieben A, Sforza F, Karim R, Coughlin K, Isaksson Vogel R, Gavioli R, McCullar V, Lenvik T, *et al.* (2015). UNC-45A is a nonmuscle myosin iia chaperone required for NK cell cytotoxicity via control of lytic granule secretion. J Immunol 195, 4760–4770.

Jilani Y, Lu S, Lei H, Karnitz LM, Chadli A (2015). UNC45A localizes to centrosomes and regulates cancer cell proliferation through ChK1 activation. Cancer Lett 357, 114–120.

Katsuno H, Toriyama M, Hosokawa Y, Mizuno K, Ikeda K, Sakumura Y, Inagaki N (2015). Actin migration driven by directional assembly and disassembly of membrane-anchored actin filaments. Cell Rep 12, 648–660.

Kiboku T, Katoh T, Nakamura A, Kitamura A, Kinjo M, Murakami Y, Takahashi M (2013). Nonmuscle myosin II folds into a 10S form via two portions of tail for dynamic subcellular localization. Genes Cells 18, 90–109.

Kovács M, Tóth J, Nyitray L, Sellers JR (2004). Two-headed binding of the unphosphorylated nonmuscle heavy meromyosin.ADP complex to actin. Biochemistry 43, 4219–4226.

Lee CF, Melkani GC, Bernstein SI (2014). The UNC-45 myosin chaperone: from worms to flies to vertebrates. Int Rev Cell Mol Biol 313, 103–144.

Limouze J, Straight AF, Mitchison T, Sellers JR (2004). Specificity of blebbistatin, an inhibitor of myosin II. J Muscle Res Cell Motil 25, 337–341.

Lin CH, Espreafico EM, Mooseker MS, Forscher P (1996). Myosin drives retrograde F-actin flow in neuronal growth cones. Neuron 16, 769–782.

Lin CH, Thompson CA, Forscher P (1994). Cytoskeletal reorganization underlying growth cone motility. Curr Opin Neurobiol 4, 640–647.

Lowery LA, Van Vactor D (2009). The trip of the tip: understanding the growth cone machinery. Nat Rev Mol Cell Biol 10, 332–343.

Medeiros NA, Burnette DT, Forscher P (2006). Myosin II functions in actin-bundle turnover in neuronal growth cones. Nat Cell Biol 8, 215–226.

Ni W, Hutagalung AH, Li S, Epstein HF (2011). The myosin-binding UCS domain but not the Hsp90-binding TPR domain of the UNC-45 chaperone is essential for function in Caenorhabditis elegans. J Cell Sci 124, 3164–3173.

Ni W, Odunuga OO (2015). UCS proteins: chaperones for myosin and co-chaperones for Hsp90. Subcell Biochem 78, 133–152.

Pollard TD, Blanchoin L, Mullins RD (2000). Molecular mechanisms controlling actin filament dynamics in nonmuscle cells. Annu Rev Biophys Biomol Struct 29, 545–576.

Price MG, Landsverk ML, Barral JM, Epstein HF (2002). Two mammalian UNC-45 isoforms are related to distinct cytoskeletal and muscle-specific functions. J Cell Sci 115, 4013–4023.

Schaar BT, McConnell SK (2005). Cytoskeletal coordination during neuronal migration. Proc Natl Acad Sci USA 102, 13652–13657.

Shi H, Blobel G (2010). UNC-45/CRO1/She4p (UCS) protein forms elongated dimer and joins two myosin heads near their actin binding region. Proc Natl Acad Sci USA 107, 21382–21387.

Spillane M, Ketschek A, Donnelly CJ, Pacheco A, Twiss JL, Gallo G (2012). Nerve growth factor-induced formation of axonal filopodia and collateral branches involves the intra-axonal synthesis of regulators of the actin-nucleating Arp2/3 complex. J Neurosci 32, 17671–17689.

Straight AF, Cheung A, Limouze J, Chen I, Westwood NJ, Sellers JR, Mitchison TJ (2003). Dissecting temporal and spatial control of cytokinesis with a myosin II inhibitor. Science 299, 1743–1747.

Suter DM, Forscher P (2000). Substrate-cytoskeletal coupling as a mechanism for the regulation of growth cone motility and guidance. J Neurobiol 44, 97–113.

Vallee RB, Seale GE, Tsai JW (2009). Emerging roles for myosin II and cytoplasmic dynein in migrating neurons and growth cones. Trends Cell Biol 19, 347–355.

Vicente-Manzanares M, Ma X, Adelstein RS, Horwitz AR (2009). Non-muscle myosin II takes centre stage in cell adhesion and migration. Nat Rev Mol Cell Biol 10, 778–790.

Vicente-Manzanares M, Zareno J, Whitmore L, Choi CK, Horwitz AF (2007). Regulation of protrusion, adhesion dynamics, and polarity by myosins IIA and IIB in migrating cells. J Cell Biol 176, 573–580.